Laser wavelength effects on ionic and atomic emission from tin plasmas

D. Campos,[a] S. S. Harilal, and A. Hassanein
School of Nuclear Engineering and Center for Materials Under Extreme Environment, Purdue University, 400 Central Drive, West Lafayette, Indiana 47907, USA

(Received 26 January 2010; accepted 19 March 2010; published online 12 April 2010)

We investigated the effects of laser wavelength on atomic and ionic emission from Sn plasmas. Plasmas were produced using planar Sn targets excited with 10.6 μm carbon dioxide (CO_2) and 1.06 μm neodymium-doped yttrium aluminum garnet (Nd:YAG) lasers. Two-dimensional spectral imaging of visible emission showed that continuum emission was significantly more intense in the CO_2 laser produced plasma (LPP) whereas line emission was considerably more extensive in the Nd:YAG LPP. Faraday cup analysis showed that ion profiles were narrower with CO_2 LPPs although they possessed higher kinetic energies. © *2010 American Institute of Physics*.
[doi:10.1063/1.3386524]

Optical lithography is rapidly approaching its physical limitations for etching sufficiently small features onto integrated circuits. To continue the trend of Moore's Law it is essential to develop a commercially viable light source in the extreme ultraviolet (EUV) regime at 13.5 nm for the next generation of lithography. The selection of 13.5 nm radiation relies on the availability of multilayer mirrors which reflect 2% bandwidth centered at 13.5 nm. Spitzer *et al.*[1] reported that tin targets irradiated by a neodymium-doped yttrium aluminum garnet (Nd:YAG) laser generated a high conversion efficiency (CE) thus suggesting that laser produced plasmas (LPPs) are a viable source for obtaining this light. For the plasma to radiate the requisite light not only must it have the correct electron temperature (~30 eV) but also it must not be so dense that the EUV photons cannot escape. Many studies have shown that the EUV emission characteristics of laser produced Sn plasmas depend strongly on a multitude of factors such as follows: target geometry,[2,3] target material, laser spot size,[4] laser wavelength,[5] etc. A suitable LPP source will require an efficient conversion of the incident laser pulse energy to EUV radiation as well as nearly complete control of debris transport.

Initially, only Nd:YAG excitation was explored thoroughly[1,2,6] for EUV source development but Tanaka *et al.*[7] found that a CO_2 provides a comparable CE thus establishing the CO_2 Sn LPP as a viable candidate for EUVL. Moreover, the CO_2 laser produces plasma that gives a narrower unresolved transition array around 13.5 nm due to its lower opacity.[5] It has since been found that CO_2 plasmas emit less debris per pulse than a Nd:YAG plasma.[8] A good comparison of atomic and ionic debris from CO_2 and Nd:YAG LPPs is very useful for ongoing EUVL source development. In this letter, we report a detailed comparison between atomic and ionic emission from plasmas produced by CO_2 and Nd:YAG lasers. For this purpose, we employed several diagnostic tools including two-dimensional (2D) spectral imaging, time and space resolved emission spectroscopy and Faraday cup (FC) analysis. In our investigation, we noticed several striking differences in the visible plasma emission features between the two plasmas.

The schematic of the experimental details is given in Fig. 1. For producing plasma, 1.06 or 10.6 μm radiation from a Nd:YAG laser with full width half maximum (FWHM) 6 ns or CO_2 (FWHM 30 ns) was used. We utilized a plasma shutter device[9] to chop the long tail of the CO_2 laser. The lasers were focused onto a planar Sn target positioned at the center of a vacuum chamber with a base pressure of $\sim 10^{-6}$ Torr using a f/35 fused silica planoconvex lens for 1.06 μm or a f/10 ZnSe meniscus lens for 10.6 μm. For performing time and space resolved optical emission spectroscopy (OES), the self-emission from the plasma was collected and imaged onto the slit of a 0.5 m spectrograph (max resolution 0.025 nm). A dove prism was inserted into the optical path for capturing two-dimensional (2D) spectral imaging. One of the exit ports of the spectrograph was coupled to an intensified charged-coupled device (ICCD) and the other exit port was coupled to a photomultiplier tube (PMT) with a 2 ns rise time. The kinetic energy of the plasma ions was measured with a FC mounted inside the chamber at a distance of 16 cm from the target point, at an angle of 10°.

Our previous studies[2,4] showed that the optimum laser pulse parameters for obtaining highest CE for CO_2 and Nd:YAG lasers are 6.0×10^9 W/cm^2 and 1.5×10^{11} W/cm^2, respectively, for a spot size of 225 and

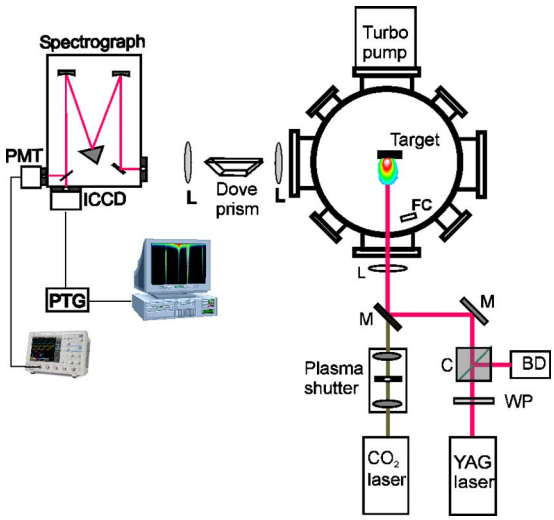

FIG. 1. (Color online) The schematic of experimental setup is given. (WP, waveplate; C, polarizing cube; BD, beam dump; L, lens; FC, Faraday cup; and PTG, programmable timing generator).

[a]Electronic mail: davedcampos@gmail.com.

 © 2010 American Institute of Physics

Author complimentary copy. Redistribution subject to AIP license or copyright, see http://apl.aip.org/apl/copyright.jsp

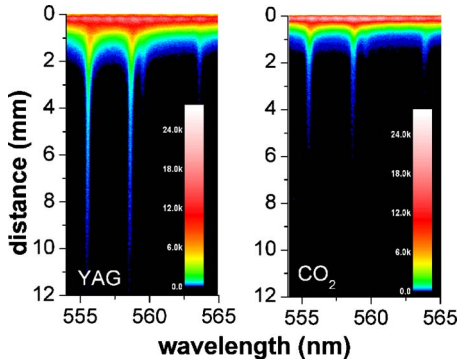

FIG. 2. (Color online) 2D spectral images of Nd:YAG (left) and CO_2 (right) plasmas. The images were taken at the onset of the plasma spark and were integrated from 0 to 2000 ns.

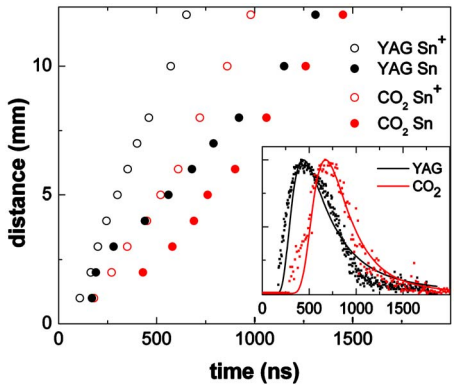

FIG. 4. (Color online) The TOF for each combination of Sn species and laser wavelength. Typical OE-TOF profiles are given in the inset.

100 μm. Hence, we used these laser intensities for the present studies. Using 2D imaging, it was possible to obtain images of the respective plasma emission spectra and compare them side-by-side with high spatial precision ($\sim$25 μm). Typical 2D spectral images recorded from Nd:YAG and CO_2 LPPs are given in Fig. 2. These images were obtained with 2 μs integration windows starting from the onset of the plasma. Figure 2 clearly shows that the extent of optical emission is significantly greater for the plasma produced by 1.06 μm irradiation. Line emission is significant until approximately 10 mm for the Nd:YAG LPP whereas line emission vanishes at approximately 5 mm for the CO_2 LPP. Despite the stronger line emission intensity in the Nd:YAG LPP, the maximum continuum intensity was found to be significantly higher for the CO_2 LPP than for the Nd:YAG LPP.

We estimated the temperature (T_e) and density (n_e) of the plasma plumes from 2D spectral imaging using the Boltzmann plot method and the Stark broadening profiles, respectively.[10] The spectroscopic parameters are obtained from Ref. 11 The time-integrated density of the Nd:YAG and CO_2 produced plasmas measured at various locations is given in Fig. 3. It is interesting to note that the electron density of the Nd:YAG LPP is consistently higher than the CO_2 LPP. This persists until the line intensity of the CO_2 LPP vanishes 5 mm. Unlike density, the temperature estimate showed hardly any variation between Nd:YAG and CO_2 produced plasmas. The estimated temperature at 0.5 and 3 mm were 1.40 and 0.80 eV for CO_2 produced plasma and 1.35 and 1.07 eV for Nd:YAG produced plasma, respectively.

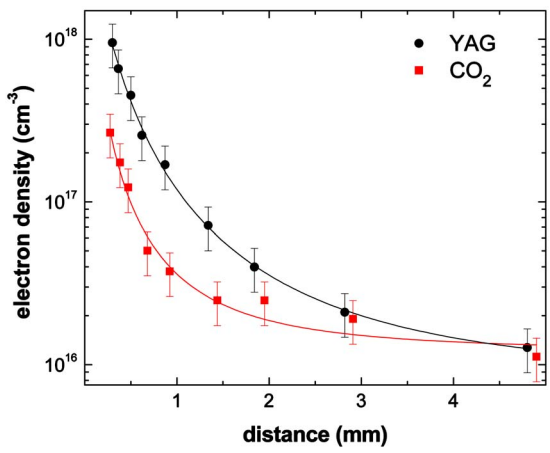

FIG. 3. (Color online) The plasma density with respect to distance from the target.

To elucidate the reasons behind the difference in the spatial extent of visible emission, we performed time and space resolved OES employing the PMT. We selected intense Sn emission lines at 317.5 nm (Sn) and at 556.2 nm (Sn^+) in our optical time of flight (OTOF) studies. An OTOF signal recorded with Sn^+ at 8 mm from the target is given in Fig. 4 inset. The velocity distributions of ions from a LPP usually follow the shifted Maxwell–Boltzmann distribution,[12] and the solid curves in Fig. 4 inset show a high correlation between the experimental data and the theoretical fit. The maximum probable arrival time of neutral as well ionic lines obtained from TOF signals are plotted against distance is given in Fig. 4. It should be mentioned that the dynamic range of PMT is several orders higher compared to the ICCD. Furthermore, to compensate for the lower line intensities from the CO_2 LPP, we used a 50 μm slit instead of 30 μm used with Nd:YAG laser. The estimated velocity of neutral Sn was 1.0×10^6 cm/s for the CO_2 LPP and 0.89×10^6 cm/s for the Nd:YAG LPP while these values for Sn^+ are 1.4×10^6 cm/s and 2.0×10^6 cm/s, respectively. It is interesting to note that the neutral emission from the CO_2 propagates approximately 10% faster whereas the singly charged state propagates 40% faster in the case of the Nd:YAG.

Our OES studies showed that the singly charged ions move much faster when the plasma is produced by 1.06 μm excitation. However, the main contributors of EUV in-band emission[5] at 13.5 nm are Sn^{9+}–Sn^{13+}. Visible emission spectroscopy is useful only for analyzing neutral and singly ionized Sn species. Therefore, a FC was employed to record ionic debris features coming from all charge-states except neutrals. Figure 5 gives representative time of flight (TOF) profiles for the ionic debris from the CO_2 and Nd:YAG LPPs along with their kinetic profiles (inset). It is interesting to note that the ion profile from the CO_2 excited plasma is much narrower than that of the Nd:YAG produced plasma. Also, despite obtaining higher kinetic energy with singly ionized species in the Nd:YAG LPP using OES, the FC ionic profiles show that the kinetic energy spectrum of the CO_2 LPP is shifted to the higher energy side. It was found that the maximum probable kinetic energy of ionic species from CO_2 LPP is approximately 2.2 keV which is about twice as energetic the Nd:YAG LPP's 1.2 keV.

The shift in the kinetic energy peak to higher energy for the CO_2 LPP can be related to observation of bright continuum emission in the spectral images. In the emission spectra, the continuum emission originates from excited, free

Author complimentary copy. Redistribution subject to AIP license or copyright, see http://apl.aip.org/apl/copyright.jsp

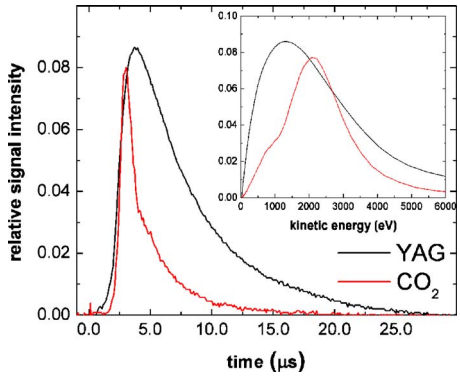

FIG. 5. (Color online) The raw Faraday cup signal given by the oscilloscope for CO_2 and Nd:YAG debris. Inset is the kinetic energy distribution for the ionic debris for each plasma.

electrons whereas line emission originates from excited, bound electrons. The CO_2 LPP's brighter continuum emission implies a larger relative population of free electrons. To get free electrons it is necessary to ionize target material, so one must therefore expect a higher degree of ionization in the CO_2 LPP versus the Nd:YAG LPP. The mean charge-state of the ions emitted from a LPP can be calculated from; $E(\text{eV})=5(Z+1)\times T_e(\text{eV})$ where E is the most-probable kinetic energy and Z is the average charge state.[13] Assuming similar T_e, it was found that the average charge states of the LPPs were approximately 8 and 14 for Nd:YAG and CO_2, respectively. It is well known that the propagation velocities of ions in a plasma are governed by space-charge effects where highly charged ions posses higher velocities. Therefore, because of its higher average charge-state, one expects the ion kinetic energy distribution from CO_2 LPP to be shifted to higher energy versus the Nd:YAG LPP which is consistent with FC ion signals.

The OES studies also showed that the extension of line emission is higher for Nd:YAG LPPs. Farther away from the target, the dominant mechanism for producing the lower-charged species is collisional three-body recombination, the rate of which is[13] given by $R_c \alpha Z^3 \ln \sqrt{Z^2+1} T_e^{-9/2} n_e^2 n_i$, where n_i is the ion density. The measured initial density[4] during the peak of the laser pulse for the CO_2 LPP near the target showed $\sim 10^{19}$ cm^{-3} which is higher than the critical density of the excitation beam. Once the plasma reaches the critical density, the remaining part of the laser beam is absorbed by the coronal expanding part of the plasma (and/or reflected by the critical density region) so one can expect more ionization in the coronal part. In comparison, previous studies[14] identical to our experimental parameters showed that the Nd:YAG LPP reaches the critical density of the 0.532 μm probe beam ($\sim 10^{21}$ cm^{-3}) which is two orders higher in magnitude compared to the CO_2 LPP. The estimated density at farther distances from the target (Fig. 3) also showed higher density for the Nd:YAG produced plasma. The rate of collisional three-body recombination is proportional to $\sim n_e^2$; thus, there is an initial four order of magnitude difference in the rates of recombination. Furthermore, as the plasma expands away from the target, the electron density drops considerably. The higher density of the Nd:YAG LPP fuels three-body recombination farther away from the target allowing the continued production of Sn and Sn^+ which are the species responsible for visible emission. This explains the farther extent of line emission in the case of the Nd:YAG LPP. The recombination effects also lead to the broader kinetic energy ion profiles due to the higher presence of distinctly charged ions for the Nd:YAG LPP. Conversely, the lower rate of recombination effects in the CO_2 LPP result in the preservation of highly charged species and thus the shift to higher kinetic energy.

The disparity between the relative velocities obtained using the FC signals and OTOF studies can be understood by considering the charge state of the ions, space-charge effects, and the disparity in the rates of three-body recombination. It should be mentioned that FC collects all ions irrespective of charge state and, again, in the case of tin, OTOF studies are limited to only singly ionized and neutral species. Because of the space charge-effects, the propagation velocity of a particular ion depends on its charge state and highly charged ions move faster. However, the higher density of the Nd:YAG LPP results in recombination effects that persist farther from the target surface. This allows the formation of lower-charged ions even at farther distances away from the target which have already been accelerated. This can be clearly seen when comparing the OTOF signals of Sn^+ where they possess higher velocity components. Therefore, we conclude that efficient recombination effects in the Nd:YAG LPP lead to faster temporal profiles for the lower-charged ions compared to CO_2 produced plasmas.

In summary, we investigated the effect of wavelength on atomic and ionic emission features of laser produced Sn plasma. We employed two important excitation laser wavelengths (1.06 and 10.6 μm) relevant to on EUVL source development. Our results indicated that CO_2 LPP posses ions with higher average charge state while recombination is found to be significantly higher in Nd:YAG LPP plasma. The narrower ion profiles in CO_2 LPPs are due to efficient coupling between laser and plasma in the coronal region. Due to higher initial electron density, the Nd:YAG LPP promotes efficient recombination leading to a higher population of lower-charged ions and neutrals.

[1] R. C. Spitzer, R. L. Kauffman, T. Orzechowski, D. W. Phillion, and C. Cerjan, J. Vac. Sci. Technol. B **11**, 2986 (1993).
[2] A. Hassanein, V. Sizyuk, T. Sizyuk, and S. S. Harilal, J. Micro/Nanolith. MEMS MOEMS **8**, 041503 (2009).
[3] S. S. Harilal, T. Sizyuk, V. Sizyuk, and A. Hassanein, Appl. Phys. Lett. **96**, 111503 (2010).
[4] S. S. Harilal, R. W. Coons, P. Hough, and A. Hassanein, Appl. Phys. Lett. **95**, 221501 (2009).
[5] J. White, P. Dunne, P. Hayden, F. O'Reilly, and G. O'Sullivan, Appl. Phys. Lett. **90**, 181502 (2007).
[6] S. Fujioka, M. Shimomura, and Y. Shimada, Appl. Phys. Lett. **92**, 241502 (2008).
[7] H. Tanaka, A. Matsumoto, K. Akinaga, A. Takahashi, and T. Okada, Appl. Phys. Lett. **87**, 041503 (2005).
[8] A. Takahashi, D. Nakamura, K. Tamaru, T. Akiyama, and T. Okada, Appl. Phys. B: Lasers Opt. **92**, 73 (2008).
[9] N. Hurst and S. S. Harilal, Rev. Sci. Instrum. **80**, 035101 (2009).
[10] S. S. Harilal, B. O'Shay, M. S. Tillack, and M. V. Mathew, J. Appl. Phys. **98**, 013306 (2005).
[11] A. Alonso-Medina and C. Colon, Astrophys. J. **672**, 1286 (2008).
[12] S. S. Harilal, C. V. Bindhu, M. S. Tillack, F. Najmabadi, and A. C. Gaeris, J. Appl. Phys. **93**, 2380 (2003).
[13] P. T. Rumsby and J. W. M. Paul, Plasma Phys. Controlled Fusion **16**, 247 (1974).
[14] Y. Tao, M. S. Tillack, S. S. Harilal, K. L. Sequoia, and F. Najmabadi, J. Appl. Phys. **101**, 023305 (2007).

Author complimentary copy. Redistribution subject to AIP license or copyright, see http://apl.aip.org/apl/copyright.jsp